Characterization of silicon micro-oscillators by scanning laser vibrometry

J. F. Vignola[a] and X. Liu
SFA Inc., 9315 Largo Drive West, Suite 200, Largo, Maryland 20774

S. F. Morse,[b] B. H. Houston, J. A. Bucaro,[c] M. H. Marcus, and D. M. Photiadis
Naval Research Laboratory, 4555 Overlook Avenue, SW, Washington, DC 20375

L. Sekaric
Cornell Center for Materials Research, Clark Hall, Cornell University, Ithaca, New York 14853

(Received 10 December 2001; accepted for publication 20 June 2002)

The dynamics of single-crystal silicon ~100 μm size rectangular paddle oscillators at room temperature have been studied using a recently developed high-resolution scanning laser vibrometer. The dynamic mechanical behavior is determined by scans of the entire device, providing both amplitude and phase spatial maps of the vibratory response. These reveal more than 16 normal modes below 500 kHz. In addition to simple translation and torsional motion, flexural modes of the paddle plate are observed. Quality factors ranging from 1×10^3 to 2×10^4 are measured and are found to be significantly lower than those expected from well-known intrinsic absorption mechanisms. The measurements reveal that there exists significant modification of the expected eigenfrequencies and mode shapes. It is speculated that this is caused by excessive undercutting of the support structure, and that the resulting energy flow into the support leads to increased oscillator loss. Indeed, some correlation is found between observed loss and energy levels resident in the supports. At frequencies where there is relatively little support motion, three-dimensional finite-element modeling accurately predicts the paddle modal behavior. [DOI: 10.1063/1.1502014]

I. INTRODUCTION

High-Q mechanical oscillators based on single-crystal silicon microfabrication technology are of great interest in a variety of applications. Examples include charge detectors,[1] radio-frequency filters,[2] magnetic resonance force microscopes,[3] and torque magnetometers.[4] Up to the present time, ultra-high-Q (10^6-10^8) have been observed only in oscillators having at least centimeter lateral dimensions, a good example of which is the so-called ''double paddle'' type.[5–7] In microelectromechanical systems (MEMS), however, Q are found to be lower than expected based on scaling considerations of fundamental loss mechanisms.[8] Indeed, recent measurements by Evoy *et al.*[9] made on 5.5-μm-square Si paddles demonstrated Q reaching only 2.5×10^3 at room temperature.

The specific cause of low Q in MEMS oscillators is not presently understood. At larger length scales, experiments[10] have shown that eliminating metal films used for capacitive driving and detection may increase Q as much as threefold. Recent experimental results on macroscale single-crystal silicon double-paddle oscillators suggest that in these high-Q oscillators the internal friction in lower-Q modes can be correlated with vibration of the supporting structure.[11] Indeed, it is for those modes with minimal coupling to the supports that moderately high Q have been obtained ($Q\sim10^6$ at 300 K). In nanofabricated single-crystal silicon wires, Q has been shown to decrease as the surface-to-volume ratio increases, suggesting that surface loss mechanisms play an increasing role as oscillator size is reduced to the nanoscale.[12] To improve our understanding of the loss mechanisms at work in silicon-based micro-oscillators in order to achieve higher-Q versions of MEMS oscillators in general, we have investigated the dynamics and loss mechanisms of some MEMS oscillators with a recently developed, high-resolution *in situ* measurement technique capable of revealing the detailed motion of both the oscillator and the supporting structures as well. In this article, we report such high-resolution (<3 μm) laser Doppler vibrometry scanning measurements made on single-crystal silicon paddle oscillators having lateral spatial dimensions in the 100 μm range. The resulting detailed information is used to identify the actual modal response of the complete structure in an attempt to understand the low-Q values seen in general for such microscillators.

II. SAMPLE PREPARATION

The oscillators were fabricated on a silicon-on-insulator (SOI) ⟨100⟩ substrate using optical lithography and Si micromachining techniques at the Cornell Nanofabrication Facility.[13] The top Si layer, which after processing makes up the oscillator and the top layer of the supporting structures, is 1.5 μm thick. The oxide layer, which is removed to produce released features, is 3 μm thick. The silicon is nominally undoped with a resistivity of 14–22 and 1–3 Ω cm for the

[a]Present address: Naval Research Laboratory, Washington, DC 20375.
[b]Present address: Department of Computer Science, Western Oregon University, Monmouth, OR 97361.
[c]Electronic mail: bucaro@pa.nrl.navy.mil

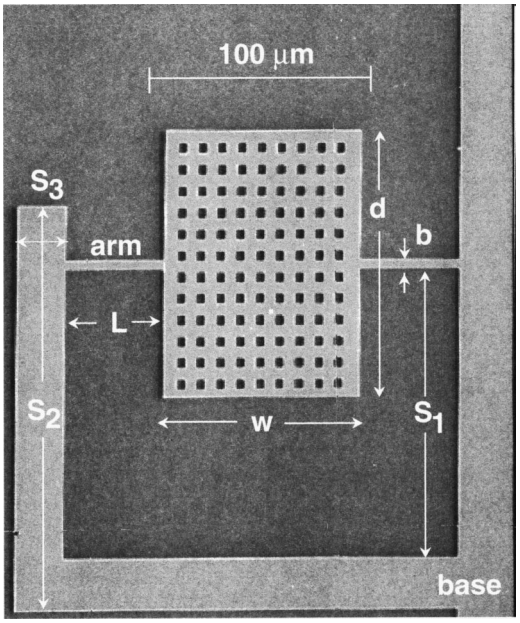

FIG. 1. Scanning electron micrograph of a single-crystal silicon paddle oscillator fabricated in SOI substrate with $d=147$ μm. An array of eight oscillators with $d\equiv 100-270$ μm was fabricated on a single wafer. Other parameters are (in μm): $w=97.8$, $L=50.9$, $b=4.15$, $S_1=130.0$, $S_2=183.8$, and $S_3=23.5$; all with thickness $h=1.5$. The oxide layer etched to release the oscillator was 3 μm.

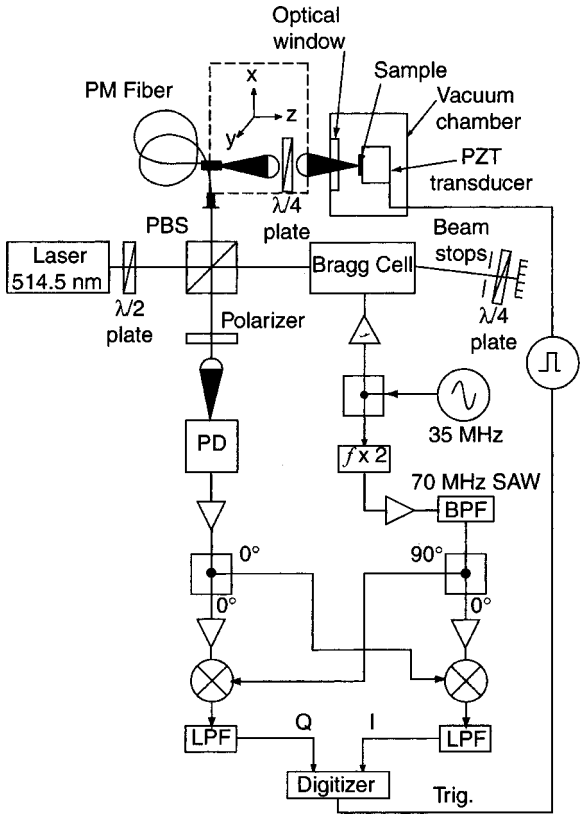

FIG. 2. Schematic diagram of the scanning laser Doppler vibrometer microscope (LDVM) system and associated demodulation setup. Notation: PBS, polarizing beam splitter; PM, polarization maintaining fiber; PD, photodetector; $f\times 2$, frequency doubler; BPF, band pass filter; SAW, surface acoustic wave; and LPF, low pass filter.

top Si and substrate, respectively. Before processing, the wafer was rotated 45° with respect to the flat so that the arms of the oscillator are parallel to the 100 direction. Eight such oscillators of differing lengths were fabricated on the same wafer. For the eight oscillators, the paddle length, d, varies from 97.6 to 268 μm (Fig. 1) while all other dimensions remain fixed: (in μm) $w=97.8$, $L=50.9$, $b=4.15$, $s_1=130.3$, $s_2=183.8$, and $s_3=23.5$. This study was focused on the oscillator having $d=147$ μm. Figure 1 is a scanning electron micrograph of this oscillator. The rectangular paddle plate was designed with 5-μm-square perforations to assist in the etching of the oxide layer under the large area of the plate.

III. MEASUREMENT APPARATUS

The scanning laser Doppler vibrometer microscope (LDVM) instrument we developed for this study is comprised of three main subsystems: The optical interferometer, the demodulator and recording electronics, and a three-axis mechanical scanner. A schematic of the system is shown in Fig. 2. The optical interferometer system is a quadrature heterodyne[14] laser interferometer assembled from both bulk and fiber-optic components. It incorporates an argon-ion laser (Spectra Physics model 2060-4 with a 514.5 nm étalon for single-frequency operation). A variable half-wave plate (Lambda Research Optics) is employed at the laser output to control the balance of power in each arm of the interferometer. The beam then passes through a polarizing beam splitter (PBS) (Lambda Research Optics, PB-12B-R-488-514). The reflected component from the PBS is vertically polarized and launched down a polarization maintaining fiber (Alcoa Fujikura SM48-P-S, 450 nm cutoff). The fiber is used to deliver light to a compact probe housing containing a pair of axial GRIN lenses (Newport Optics, GPX-043 AR 14) separated by a quarter-wave plate (Lambda Research Optics, WP-12-CQ-M-4-514.5). The light then passes through the optical window of a vacuum chamber to the sample surface. For the measurements reported here, the typical spot size is 2.5 μm in diameter, and the typical power levels are kept below 0.1 mW in order to insure minimal sample heating. On the return path, the reflected light from the sample passes through the GRIN lenses and quarter-wave plate assembly, thereby achieving a rotation of 90° relative to the input. This rotation insures horizontal polarization and maximum transmission through the PBS to the photodetector. The GRIN lenses minimize spherical aberration so that a diffraction-limited spot can be achieved. These optical elements along with the optical fiber are assembled into a compact housing mounted to a three-axis positioning stage.

The transmitted beam through the PBS comprises the reference beam of the interferometer. It passes through a 35 MHz Bragg cell (Isomet, Acouto-Optic modulator model 1201E) and quarter-wave plate (Lambda Research Optics, WP-12-CQ-M-4-514.5), where it is rotated 45° relative to the horizontally polarized incident light. This is done in order to impose circular polarization on the reference beam. A mirror is aligned to retroreflect the first-order diffracted beam back along this path to the Bragg cell and the PBS. As a result, the polarization rotation and frequency modulation of the reference beam take place twice; thus, the reference beam

is up-shifted 70 MHz and rotated 90° relative to the incident beam.

Both the frequency-modulated reference beam and the reflected signal from the sample surface pass back through the PBS, a Glan Thompson polarizer (Melles Griot 03PTH001/A), and are collected at a ~1 GHz avalanche photodiode receiver (New Focus 1601AC). The polarizer serves to insure a common polarization upon mixing of the two beams.

A hybrid analog–digital approach is employed for the demodulator and recording subsystem. The photodetector contains a frequency-modulated (FM) electrical signal carrying a phase signal that is the dynamic surface displacement of the target normalized to the wavelength of light. The photodiode voltage can be written as[14]

$$V_{\text{sig}} = V \sin\left(\omega_b t + \frac{d(t)}{4\pi\lambda} + \langle \phi(t) \rangle \right) + V_{\text{noise}},$$

where V is a constant, ω_b is the frequency shift due to two passes through the Bragg cell, $d(t)/4\pi\lambda$ is the phase modulation due to the out-of-plane displacement of the sample surface referenced to the wavelength of the laser (λ), $\langle \phi(t) \rangle$ is the laser phase noise, and V_{noise} is the noise associated with the photodiode and receiver system. The dominant source of noise in this system is associated with the phase noise of the laser and determines the minimum detectable level (4×10^{-5} nm/$\sqrt{\text{Hz}}$). The maximum displacement for these measurements is approximately 5 nm. It should be pointed out that this system is capable of measurements up to ~500 MHz for the subwavelength surface displacements typically associated with MEMS resonator devices.

The phase-modulated signal plus noise is extracted using a hybrid analog–digital method. The front end of the demodulator (Fig. 2) employs an analog stage (various Mini-Circuits, Inc., components) to extract the quadrature components at the base band of the system.[14] These are digitized, and simple processing is performed to determine the arctangent (i.e., phase) of the signal. This is accomplished by generating a pair of electrical reference signals phase locked to the Bragg cell drive signal and phase shifted 90°. This, in turn, is done by tapping off the 35 MHz Bragg cell electrical drive signal, doubling it, filtering it, splitting it, and retarding one of the outputs by 90° (Fig. 2). These two reference signals are then individually mixed with the output of a splitter fed by the FM signal from the photodetector. The two signals are subsequently captured with a 14 bit wavelength digitizer (Datel model PCI-416N). The displacement plus noise normalized to the wavelength of the laser light is then found as the output of a four-quadrant arctangent routine on a computer, viz. $\tan^{-1}(I/Q)\lambda/4\pi n$, where I and Q are the two quadrature signals (Fig. 2), λ is 514.5 nm, and n is the index of the medium where the Doppler shift occurred ($n=1$).

IV. EXPERIMENTS

Scans were performed on each of the oscillators at room temperature. A mechanical scanner subsystem was used to precisely position the probe relative to the sample. For these experiments, the silicon wafer sample was mounted with carbon tape on a 500 kHz ultrasound transducer (K-B Aerotec 0.5 MHz-Alpha) that was in turn mounted in the vacuum chamber. The vacuum was maintained to <0.1 mTorr to eliminate acoustic radiation damping. Scanning motion takes place in air outside the vacuum chamber with the probe head portion of the vibrometer mounted on a three-axis scanning stage (Dadel 8122P-0414) with incremental optical linear encoder feedback with 100 nm resolution (Dynamic Research Corporation, model LB).

In order to study the motion of the entire structure, the scan area was made large enough to include the support regions. For the measurements reported here, the probe was scanned over the paddle and boundary in 10 μm steps. A step size of 2 μm was used for the supporting arms. The sample locations on the oscillator plate region were selected to miss the perforations. The wafer was attached to a pieozoelectric transducer crystal driven by a linearly swept frequency chirp from 1 to 500 kHz with a temporal length of 4 μs. A typical measurement included acquisition of the associated transient response at 3141 locations with 100 averages per point. These records were then windowed (Hanning window) and transformed by fast Fourier transform. With respect to the oscillator upon which we concentrated, the magnitude and phase maps for eight of the more prominent resonances below 500 kHz are plotted in Fig. 3. Nodal lines appear as deep blue and large amplitude regions as red.

Four of the six lowest-frequency modes observed [Figs. 3(a), 3(b), 3(c), and 3(e)] are principally ''rigid-body-'' type modes of the paddle plate, i.e., the plate remains planar while the arms and supports undergo bending. Modes (d) and (f)–(h) display considerable flexural plate motion. In particular, (f), (g), and (h) resemble the classic modes of a plate with four free boundaries.

V. DISCUSSION

In addition to motion of the oscillator plate itself, the scan readily reveals motion in the support structure. The considerable motion of the top Si support layer (the arm appearing on the left in Fig. 3) suggests that the SOI underlying these structures has been undercut by the etching process. Scans of the other oscillators reveal similar mode structure as in Fig. 3, but with different resonance frequencies, which are consistent with predictions based on the overall change in the plate dimensions.

A finite-element model, created using the program Sara3D,[15] was employed to predict the dynamic behavior expected for the oscillator assuming it was tied to a rigid support structure. The model used orthotropic silicon material properties.[16] It required 4040 solid elements and discretization of approximately two elements per perforation and two elements through the thickness. The excitation was a harmonic displacement applied to the oscillator at one of the plate corners. For modes where the plate vibrations have nodes at the attachments minimizing coupling to the supports, the calculation accurately predicts both the frequency and mode shape experimentally observed. For example, for

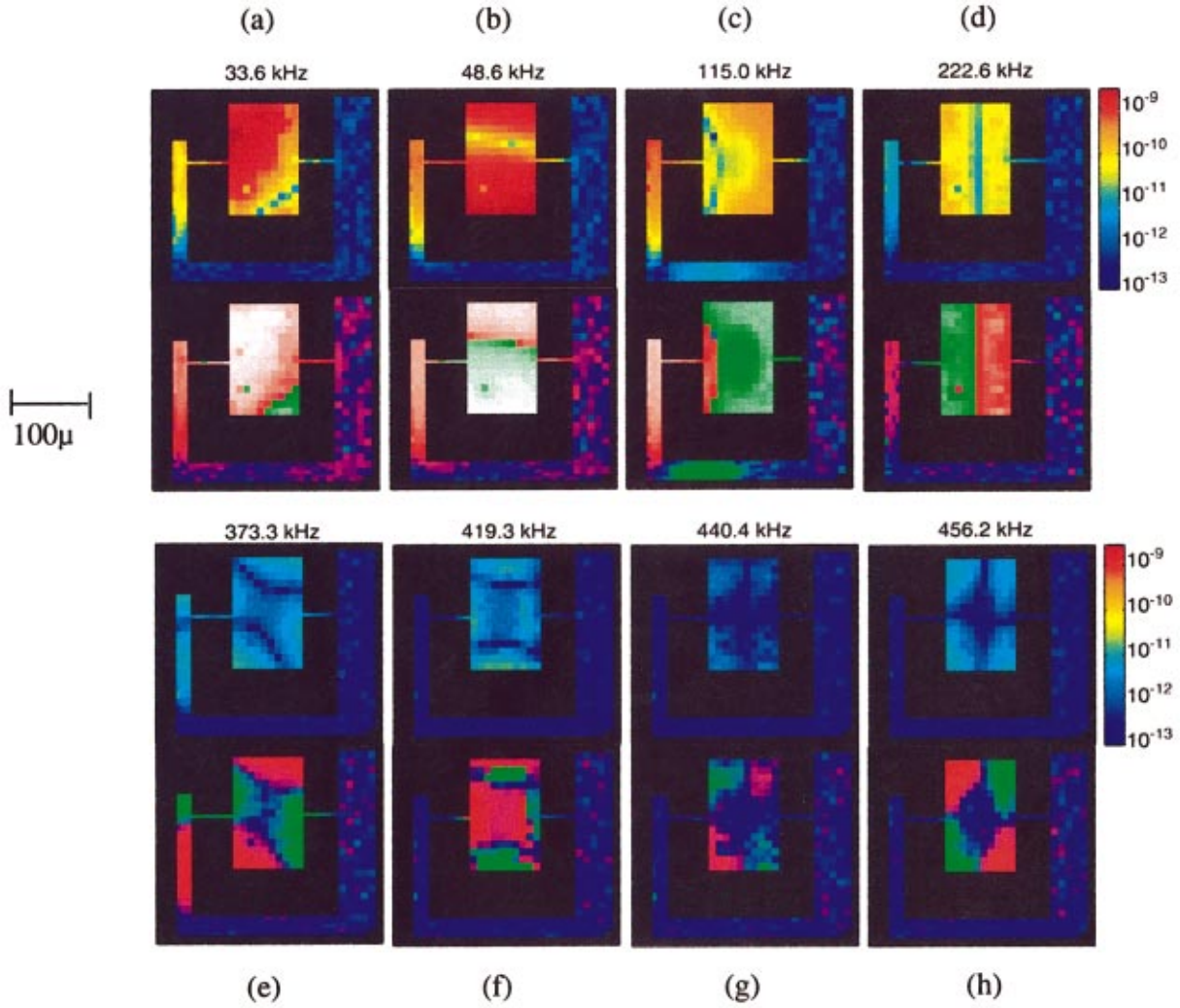

FIG. 3. (Color) LDV scan (amplitude, upper; phase, lower) of the paddle oscillator and supporting structure decomposed by frequency. The displacement of 8 of the 19 modes observed below 500 kHz are shown with the amplitude color scale in meters and the phase scale going from red ($+\pi$) to green ($-\pi$). Modes (a), (b), (c), and (e) are rigid-plate-type modes, while (d) and (f)–(h) involve considerable plate bending. Mode (d) is similar to the fundamental mode of a beam clamped at both ends. Mode (h) exhibits the largest Q of all modes observed.

the [2,2] mode of Fig. 3(h), the measured and predicted frequencies are within 1%. For the resonances in which the oscillator is expected to have significant motion near the support, the modal behavior and frequency actually observed were not predicted well. It is reasonable to assume that the change in mode structure and eigenfrequencies is, in fact, due to excessive undercutting of the support structure.

Table I lists Q^{-1} determined at the frequencies displayed in Fig. 3 together with some additional lower-amplitude resonances. Here, Q range from about 1×10^3 to 2×10^4. Since our technique provides detailed spatial maps of the vibratory response, we are able to determine other useful oscillator parameters. For example, also shown in Table I is the kinetic energy in the bottom support and the attachment structure normalized to the total kinetic energy as determined from the LDVM scans by integrating the square of the velocity (v^2) over the pertinent structures. This metric allows us to test for a quantitative correlation between the amount of kinetic energy near the attachment points to the base structure and the system loss[11] (Q^{-1}). One observation that can be made in Table I is that for all the modes having $Q>10^4$, the energy ratio is quite low, i.e., no more than several tenths of 1%. Conversely, the very lowest Q (those $\sim10^3$) have relatively high ratios, i.e., on the order of 10%. In between these high and low values of Q, there is a less clear correlation of Q and the energy ratio.

The known intrinsic absorption mechanisms for crystalline silicon do not account for these measured values of loss even for those modes exhibiting the highest Q. Specifically, for phonon–phonon interaction[17] caused by crystal lattice anharmonicity one would expect at frequency f to observe $fQ\sim10^{14}$ Hz; for thermoelastic dissipation induced by longitudinal inhomogeneous dynamic strains[18] one would anticipate $fQ\sim10^{16}$ Hz; and for thermoelastic dissipation associated with transverse strains[19] $fQ\sim10^{12}$ Hz is expected. We, therefore, predict that these internal dissipation mechanisms would result in much lower losses than those shown in Table I. Indeed, our highest fQ product is found for the highest frequency, lowest loss mode and is $fQ=8.5\times10^9$ Hz. This is two orders of magnitude below the limit set by ther-

TABLE I. Mode frequencies, measured Q's, and energy ratio (v^2 level over the support structure divided by v^2 over entire structure).

Mode frequencies	$Q\times10^{-3}$	Energy ratio$\times10^{2}$
33 600	10.6	0.00099
48 645	17.3	0.00061
62.836	1.1	11.6
72 021	1.2	11.3
82 916	1.2	12.7
87 891	2.7	4.9
115 021	14.2	0.0015
150 665	2.7	21
189 056	2.1	17.2
222 656	1.7	0.72
310 516	12.5	0.17
373 383	9.0	0.016
419 647	11	0.061
441 315	9.0	1.2
456 360	18.6	0.0033

moelastic dissipation. We thus speculate that for all the modes of this oscillator, the observed Q is in fact controlled by energy flow through the undercut supports and through the attachments, with the highest-Q modes being those that are most isolated from the supports because of their mode shape. For the data reported here the [2,2] mode at 456 kHz has the lowest measured loss, which is consistent with the small force moment expected for this mode at the attachment of the plate to the support [Fig. 3(h)]. It is anticipated that a modification of the design of these devices that both immobilizes the support structure by eliminating undercutting and also minimizes the transfer of energy to the attachments could result in the observation of Q controlled by intrinsic thermal elastic dissipation. This should result in an increase in the measured Q by as much as two orders of magnitude. Work is in progress focused on these goals.

ACKNOWLEDGMENT

This work was supported by the Office of Naval Research.

[1] A. N. Cleland and M. L. Roukes, Nature (London) **392**, 160 (1996).
[2] C. T. C. Nguyen, *Proceedings of the IEEE International Symposium on Circuits and Systems* (IEEE, Hong Kong, 1997), p. 2825.
[3] Z. Zhang, P. C. Hammel, M. Midzor, M. L. Roukes, and J. R. Childress, Appl. Phys. Lett. **73**, 2036 (1998).
[4] R. D. Biggar and J. M. Parpia, Rev. Sci. Instrum. **69**, 3558 (1998).
[5] R. N. Kleinman, G. K. Kaminsky, J. D. Reppy, R. Pindak, and D. J. Bishop, Rev. Sci. Instrum. **56**, 2088 (1985).
[6] B. E. White, Jr. and R. O. Pohl, Mater. Res. Soc. Symp. Proc. **356**, 567 (1995).
[7] X. Liu, B. E. White, Jr., R. O. Pohl, E. Iwanizcko, K. M. Jones, A. H. Mahan, B. N. Nelson, R. S. Crandall, and S. Veprek, Phys. Rev. Lett. **78**, 4418 (1997).
[8] V. B. Braginsky, V. P. Mitranov, and V. I. Panov, *Systems with Small Dissipation* (University of Chicago Press, Chicago, 1985).
[9] S. Evoy, A. Olkhovets, L. Sekaric, J. M. Parpia, H. G. Craighead, and D. W. Carr, Appl. Phys. Lett. **77**, 2397 (2000).
[10] X. Liu, E. J. Thompson, B. E. White, Jr., and R. O. Pohl, Phys. Rev. B **59**, 11767 (1999).
[11] X. Liu, S. F. Morse, J. F. Vignola, D. M. Photiadis, A. Sarkissian, M. H. Marcus, and B. H. Houston, Appl. Phys. Lett. **78**, 1346 (2000).
[12] D. W. Carr, S. Evoy, L. Sekaric, H. G. Craighead, and J. M. Parpia, Appl. Phys. Lett. **75**, 920 (1999).
[13] D. W. Carr and H. G. Craighead, J. Vac. Sci. Technol. B **15**, 2760 (1997).
[14] C. B. Scruby and L. E. Drain, *Laser Ultrasonic Techniques and Applications* (Hilger, Bristol, 1990), pp. 76–147.
[15] H. Allik *et al.*, Sara3d users manual, Report No. NL-358, BBN Systems and Technologies, New London, CT (1992).
[16] G. Simmons and H. Wang, *Single Crystal Elastic Constants and Calculated Aggregate Properties: A Handbook*, 2nd ed. (MIT, Cambridge, MA, 1971), p. 85.
[17] H. E. Bommel and R. Dransfeld, Phys. Rev. **117**, 1245 (1960).
[18] L. D. Landau and E. M. Lifshitz, *Theory of Elastisity* (Nauka, Moscow, 1965).
[19] C. Zener, *Elasticity and Anelasticity of Metals* (University of Chicago Press, Chicago, 1948).